scientific reports

Check for updates

OPEN

Organ-based tumor distribution for predicting prognosis in small-cell lung cancer using fluorodeoxyglucose positron emission tomography/computed tomography

Jiwoo Park[1], Soo Ho Ahn[1], Jae-Hoon Lee[2], Young Han Lee[1,3]✉ & Arthur Cho[4]✉

To validate and compare conventional metabolic tumor burden measurements with comprehensive metabolic tumor distribution patterns using [^{18}F] fluorodeoxyglucose positron emission tomography/computed tomography (FDG PET/CT) to predict small-cell lung cancer (SCLC) prognosis. This retrospective study included 520 patients with SCLC (mean age ± standard deviation, 67 ± 5.6 years; 84.8% men) who underwent PET/CT for staging. Of these, 364 scans were used for training (*n* = 291) and internal (*n* = 73) tests, while 156 other scans were used for external testing. Clinical data (age, sex, and stage) were reviewed. Volumes of interest were manually drawn using a threshold standard uptake value of 2.5 for total lesion glycolysis (TLG) for all tumor lesions on PET. TLG with distribution (TLGd) and organ-based tumor distribution (metastasis in organs, METAORG) was analyzed from CT-based automatic organ segmentation and overlaid on PET. Four survival prediction models (event and duration) were developed using a Random Forest classifier: (1) clinical factors, (2) tumor TLG, (3) TLGd and METAORG, and (4) combined models. The top 11 features were selected for survival duration prediction included clinical factors (age and stage), TLG, five TLGd radiomics features, and three METAORG features (axial and peripheral skeletal distribution patterns and the liver distribution pattern). In the internal test, C-indices for overall survival were 0.611, 0.592, 0.721, and 0.753 for tumor TLG, clinical, METAORG, and combined model, respectively. External test C-indices were 0.637, 0.326, 0.706, and 0.740, respectively. The combined model, which incorporated tumor distribution information such as TLGd and METAORG, demonstrated the highest predictive power for both test sets. The combined model outperformed the other models in predicting survival. Application of tumor distribution (TLGd and METAORG) to whole-body tumor distribution pattern analysis shows promise for improving prognosis evaluation, with advantages of quantifiable metastasis stratification.

Keywords Small-cell lung cancer, Quantitative imaging, [^{18}F] FDG PET/CT, Tumor burden, Tumor distribution

Lung cancer is one of the most common malignancies and the leading cause of cancer-related deaths worldwide[1–3], with a 5-year survival rate < 7%[4–10]. Recent developments in new treatment modalities, such as immunotherapy and targeted therapy, have substantially increased patient survival. Despite advances in treatment modalities and the increased availability of advanced imaging modalities, the categorization and quantification of metastases

[1]Department of Radiology, Research Institute of Radiological Science, Center for Clinical Imaging Data Science (CCIDS), Yonsei University College of Medicine, 50-1 Yonsei-ro, Seodaemun-gu, Seoul 03722, South Korea. [2]Department of Nuclear Medicine, Gangnam Severance Hospital, Yonsei University College of Medicine, Seoul, South Korea. [3]Institute for Innovation in Digital Healthcare, Yonsei University, Seoul, South Korea. [4]Department of Nuclear Medicine, Yonsei University College of Medicine, 50-1 Yonsei-ro, Seodaemun-gu, Seoul 03722, South Korea. ✉email: sando@yuhs.ac; artycho@yuhs.ac

remain limited. As treatment modalities advance, imaging modalities must also advance to reflect treatment response and evaluate overall survival correctly. Most patients with small-cell lung cancer (SCLC) present with metastasis at the time of clinical diagnosis[11]. The location of metastasis substantially impacts prognosis, with the liver, brain, bone, and lungs being common sites associated with poor overall survival[12,13]. Additionally, the pattern of metastasis distribution is crucial[14,15]. The distance from the primary lesion to the furthest metastatic site, distance from the mediastinum, or even the metastasis pattern within a specific organ has been shown to correlate with patient prognosis[16–19]. However, these imaging factors are currently only used qualitatively by clinicians. Without quantifiable analysis, it is challenging to incorporate these findings consistently into treatment response evaluations. Therefore, developing automated imaging tools that quantify metastasis extent, distribution, and organ involvement is essential to fully leverage advances in treatment modalities[11–19].

Studies using ^{18}F-fluro-2-deoxy-glucose positron emission tomography/computed tomography ([^{18}F] FDG PET/CT) have shown that the total tumor burden, either the metabolic tumor volume (MTV) or total lesion glycolysis (TLG), is also an important factor in patient prognosis[10]. Recent advances in artificial intelligence have allowed the reliable automatic delineation of patient organs[20–22]. As CT scans in PET/CT are used for attenuation correction, CT-based regions of interest can be transferred to PET scans to evaluate metabolic information[23]. We propose using this method to evaluate whole-body tumor involvement patterns using [^{18}F] FDG PET/CT to provide clinicians with more comprehensive data that reflects metastatic organ involvement and tumor organ distribution patterns. Instead of using radiomics to evaluate intralesional heterogeneity within a single tumor, we applied a radiomics analysis method by considering the patient as an organ/entity and evaluating the tumor distribution patterns for all measurable malignant lesions. We hypothesized that this new application of radiomics metrics will predict patient prognosis more accurately than simple tumor burden measurements such as TLG PET metrics. The potential result is a single-stop evaluation of tumor burden and metastasis distribution for prognosis and treatment response evaluation.

This study aimed to develop and validate predictive models based on clinical factors, tumor burden (TLG), METAORG (METAstasis distribution pattern in ORGan), and total lesion glycolysis with distribution (TLGd) using [^{18}F] FDG PET/CT for survival analysis of patients with SCLC.

Materials and methods

Patient cohort

The study protocol adhered to the tenets of the Declaration of Helsinki and was approved by the Institutional Review Board of Severance Hospital (IRB no. 4-2024-0748). PET/CT images were obtained during standard patient care; thus, the institutional review board waived the need for informed consent from patients owing to the study's retrospective design. All procedures were performed in accordance with relevant guidelines/regulations.

We reviewed electronic medical records of patients diagnosed with SCLC between January 2009 and December 2022 at Severance Hospital. During this period, a total of 834 patients underwent [^{18}F] FDG PET/CT at our institution for the assessment of metastatic disease. The inclusion criteria were as follows: (1) patients who underwent baseline [^{18}F] FDG PET/CT for pretreatment staging work-up; and (2) those with an initial pathologic confirmation of SCLC obtained through biopsy, conducted within ± 1 month of the PET/CT scan. The exclusion criteria were: (a) patients who did not receive systemic or local treatment after PET/CT scan ($n = 99$); (b) those with inadequate PET/CT image quality for analysis ($n = 23$ from chemotherapy [CTx] or chemotherapy and radiotherapy [CCRTx] group, 63 from immunotherapy and chemotherapy [IO + CTx] group); (c) those with a history of another active malignancy ($n = 39$); and (d) patients who survived 3 days or less after the PET/CT scan ($n = 90$). Finally, a total of 364 patients were included in the analysis. The internal cohort (Shinchon Severance Hospital) dataset was randomly divided into a training set ($n = 291$) and an internal test set ($n = 73$) in an 80:20 ratio.

For the external test set, 156 PET/CT scans were collected from our sister hospital (Gangnam Severance Hospital) between January 2008 and December 2023 using the same criteria. A detailed flow diagram of the patient selection process is shown in Fig. 1.

Electronic medical records were reviewed for demographic and clinical information, such as age, sex, initial stage (limited disease [LD] vs. extensive disease [ED]), treatment method (CTx, CCRTx, and IO + CTx), and survival time. Patient age was categorized into decades. Overall survival time was defined as the interval between the PET/CT scan and expiration date. We used the Bonferroni post-hoc analysis to evaluate differences between the training, internal test, and external test sets. The log-rank test was used to compare the differences in survival among the three sets.

FDG-PET/CT

All PET/CT scans were performed using GE Discovery 710 PET/CT (GE Healthcare, Chicago, IL, USA; $n = 93$), GE Discovery 600e PET/CT (GE Healthcare; $n = 131$), or Siemens Biograph True point PET/CT 40 (Siemens Healthineers, Erlangen, Germany; $n = 140$) at Shinchon Severance Hospital and Siemens Biograph True point PET/CT 40 (Siemens Healthineers; $n = 156$) at Gangnam Severance Hospital. The patients fasted for at least 6 h before imaging, and glucose levels in the peripheral blood were confirmed to be < 140 mg/dL prior to [^{18}F] FDG injection. An [^{18}F] FDG dose of 3.7 ± 0.3 MBq/kg was administered intravenously 1 h before image acquisition, in accordance with our institutional protocol. After initial low-dose CT (Discovery Series PET/CT; 60 mA, 120 kVp; or Biograph TruePoint 40, 36 mA, 120 kVp), a standard PET protocol was used to scan each patient from the neck to the proximal thighs, with an acquisition time of 3 min per bed position in the three-dimensional mode. Images were reconstructed using ordered subset expectation maximization (Discovery Series: 2 iterations, 16 subsets; Biograph TruePoint 40: 3 iterations, 8 subsets). A Gaussian filter was applied, with a 4 mm full width at half maximum for Siemens Biograph True point 40 PET/CT and 5 mm for the Discovery Series PET/CT.

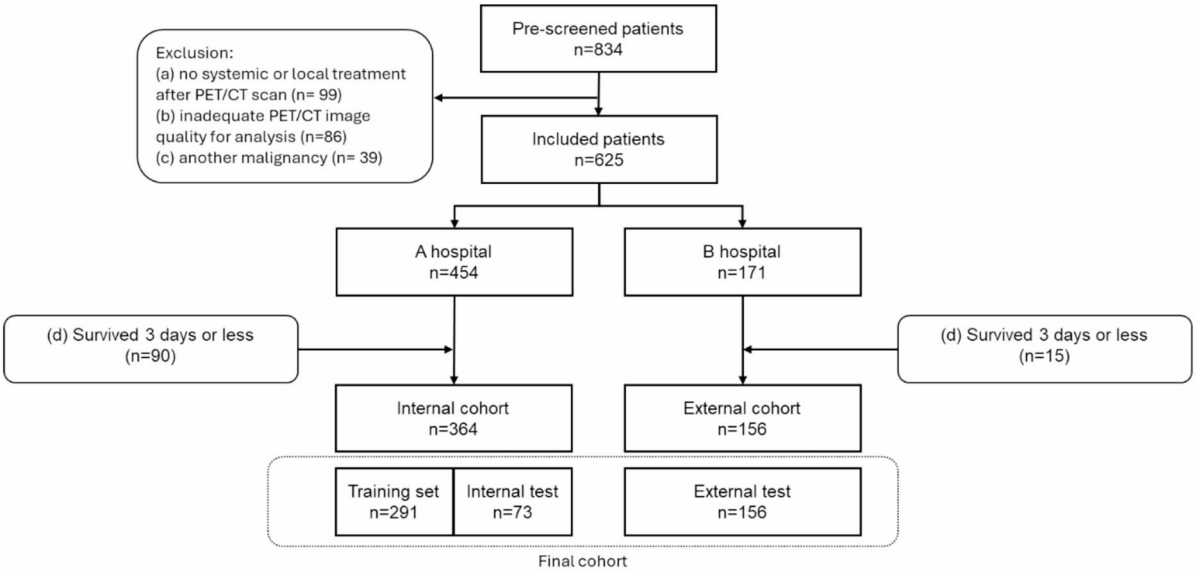

Fig. 1. Flowchart for patient selection and development of datasets.

Manual tumor segmentation (TLGd) and automatic organ segmentation (METAORG)

PET and CT scans were exported in the Digital Imaging and Communications in Medicine format and converted to the NIFTI format. In the image preprocessing step, the PET images were resampled to obtain the same resolution as that of the CT images using the SimpleITK library. Linear interpolation was used to maintain consistency between CT and PET images.

For tumor segmentation, volumetric tumor regions were semi-automatically segmented on PET by an experienced nuclear medicine physician (A.C., 18 years of experience; J-H.L., 20 years of experience) using 3D Slicer software (http://www.slicer.org)[24]. A spherical volume of interest (VOI) that encased the whole primary lesion was drawn, and a maximum standard uptake value (SUVmax) of 2.5 was used as an absolute threshold to define MTV. Active atelectasis, defined as collapsed lung parenchyma with increased [^{18}F] FDG uptake, was carefully distinguished from pulmonary tumor lesions using contrast-enhanced CT correlation and excluded during manual segmentation. For lymph nodes, all lesions with SUV > 2.5 were included in the total tumor volume irrespective of size, such that even normal-sized nodes with moderate uptake above this threshold were incorporated. TLG was calculated as MTV × SUVmean. This process was repeated for all measurable metastatic lesions, and the final MTV and TLG values were calculated as the sum of all tumor lesions. As this is routinely used in most studies, we referred to these metrics as conventional PET metrics in our study. Multiple tumors (primary tumors, lymph nodes, metastases) were grouped into one segment using the 3D Slicer software and overlaid on the PET scan; radiomics features were extracted to evaluate tumor distribution patterns in the entire body, regardless of organ involvement. We named this method total lesion glycolysis with distribution (TLGd). This radiomic feature only evaluates the spatial tumor distribution patterns in the entire body, regardless of organ involvement.

Next, we evaluated individual organ-specific tumor involvement using the following methods and defined this as an organ-based tumor distribution (METAORG). Total METAORG was defined as segmentation of the entire organ (e.g., whole liver, whole skeleton) on CT without separately isolating tumor lesions. Because FDG uptake is normally homogeneous in these organs, focal areas of increased uptake within the organ mostly represent metastatic involvement. Radiomics features derived from these whole-organ VOIs therefore reflect the distributional pattern of metastasis within each organ, rather than simple aggregate metabolic burden. First, the organs were automatically segmented using TotalSegmentator[25,26] for CT-based VOI generation. The following eight major organs were selected for radiomics and tumor involvement evaluation: the liver, spleen, axial skeleton, peripheral skeleton, core muscles, adrenal glands, thyroid, and lungs. TotalSegmentator identifies individual muscles and skeletal bones; however, to evaluate metastasis distribution patterns in the axial or peripheral skeleton, we grouped the C-, T-, and L-spine and sacrum as the axial skeleton and the bilateral proximal extremities, bilateral scapula, and pelvic bone as the peripheral skeleton. This was repeated for the individual muscles that were delineated using TotalSegmentator. We then used this CT-based VOI for PET analysis by transferring it onto PET for radiomics feature extraction.

Radiomics feature extraction

Radiomics features were extracted for TLGd and METAORG using the PyRadiomics library. Feature extraction for tumor-only VOI measurements was performed routinely without modifying the VOI. In the case of METAORG, two sets of TotalSegmentator-generated VOIs were generated because of the variable levels of [^{18}F] FDG uptake in each organ. We used TotalSegmentator native CT-based organ segmented VOIs (total METAORG) and modified them by applying a cut-off SUV value of 2.5 or higher (high METAORG). Therefore,

two types of features were extracted for METAORG: radiomic features of the total METAORG and those of the high (SUV > 2.5) METAORG. The extracted features were limited to the original features, with a total of 214 radiomics features per organ or lesion (107 total, 107 high). Missing feature values were estimated using mean imputation. A total of 1,984 features, including clinical features (age, sex, and initial stage), (conventional) tumor-only PET metrics (TLG), TLGd radiomics features, and METAORG radiomics features, were used to build survival prediction models (survival duration using a Random Survival Forest [RSF] survival event using a Random Forest classifier). A summary of the evaluated radiometric features is shown in Fig. 2.

Feature selection and development of a survival duration prediction model

Feature selection was performed using the RSF model to develop a survival duration prediction model. This model used survival status by considering survival duration. Of the 1,984 features, the permutation feature importance evaluation and Least Absolute Shrinkage and Selection Operator (LASSO) method were used to select 11 features. The optimal hyperparameters for the RSF model were determined using a Grid Search, and five-fold cross-validation was used to select the best parameters. The key tuning parameters included n_estimators, max_features, and min_samples_split.

Feature selection and development of a survival event model

A survival event model was developed using the Random Forest classifier. Initially, 88 features were selected from a total of 1,984 features using LASSO. The Random Forest feature importance was then applied, resulting in the final selection of 37 features used to build the classification model. Hyperparameter optimization of the Random Forest model was performed using Grid Search and 10-fold stratified cross-validation. The key tuning parameters included n_estimators, max_depth, and min_samples_leaf.

Survival model evaluation

The performances of the survival duration and event prediction models were validated using internal and external test data. To evaluate the survival prediction and classification models, the performances of models built with different feature sets were compared: conventional PET metric (TLG), clinical, radiomics (TLGd, total METAORG, high METAORG), TLG + clinical, TLG + radiomics, clinical + radiomics, and combined model (TLG + clinical + radiomics).

The survival prediction model was evaluated using the C-index, Cox proportional hazards model, and Kaplan–Meier survival curve analysis. Statistical significance was determined using the log-rank test. For survival analysis, Kaplan–Meier curves were generated using the risk scores predicted by the combined model

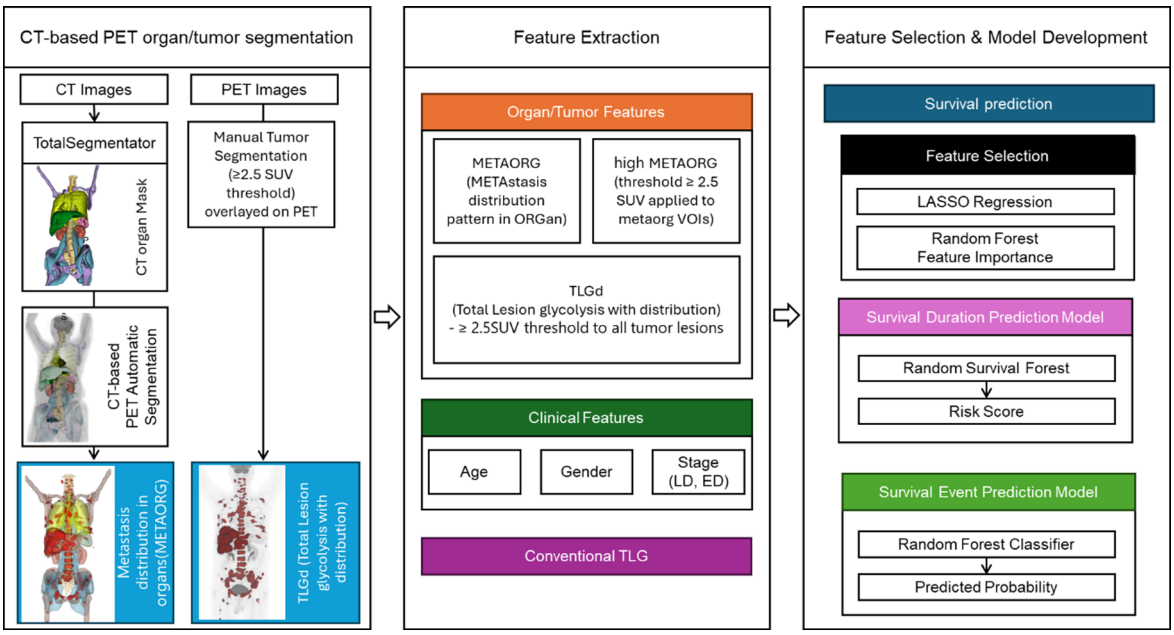

Fig. 2. Flow diagram for machine learning models. All tumor lesions were manually drawn for total lesion glycolysis (TLG) and TLG with distribution using radiomics (TLGd). Computed tomography (CT)-based organ delineation was performed using TotalSegmentator and transferred to positron emission tomography (PET) data for metastasis distribution analysis (METAORG). Note that the whole-organ VOIs (e.g., whole-liver segmentation for METAORG) were used only for distributional feature extraction, whereas TLG and TLGd were derived exclusively from tumor lesion VOIs (SUV > 2.5 threshold or manual delineation). For example, in the lower left images, the whole-liver VOI is shown as part of the METAORG analysis, and within it, metastatic lesions are also segmented (multiple spherical VOIs) for clarity. Next, feature extraction was performed, and two models were developed based on survival event alone (survival event prediction model) or overall survival including survival time (survival duration prediction model).

(TLG + clinical + radiomics features). The patients were classified into high- and low-risk groups based on risk scores above or below the median score.

For the survival event model, performance metrics, such as the area under the receiver operating characteristic curve (AUC), accuracy, precision, recall, and F1 score were used to evaluate each model. A flow diagram of the machine learning models is shown in Fig. 2.

Statistical analysis

The significance level was set at $p < 0.05$. One-way analysis of variance was used to analyze differences in continuous variables among the training, internal test, and external test sets, while chi-square tests were applied to compare categorical variables. Post-hoc analyses were conducted for variables with p-values < 0.05. For continuous variables, Tukey's honest significant difference test was used to identify specific group differences. For categorical variables, pairwise comparisons were performed using the chi-square test with Bonferroni adjustment for multiple comparisons.

Results

Patient cohort and clinical features

The characteristics of the 520 enrolled patients with SCLC are summarized in Table 1. The average age of the patients was 66.9 ± 9.6 years, with a predominance of men (441/520, 84.8%). The average follow-up period was 16.6 ± 20.5 months. Among surviving patients, the average survival time was 34.7 ± 34.2 months, compared to 12.3 ± 12.1 months for expired patients. There was no significant difference in survival based on age (survival, 65.8 ± 8.3 vs. death, 67.2 ± 9.8; $p = 0.169$). However, women had a significantly higher survival rate (26/79, 32.9% vs. 74/441, 16.8%, $p = 0.001$) than did men. Additionally, when analyzing the entire cohort, the CTx group had a lower survival rate (51/340, 15%) compared to that of the CCRTx (19/73, 26%) and IO + CTx (30/107, 28%, $p = 0.003$) groups. Patients with LD had a significantly higher survival rate than those with ED (61/135, 45.2% for LD; 39/385, 10.1% for ED; $p < 0.001$).

Regarding conventional PET metrics, patients who expired during the follow-up period had significantly higher values for SUVmax, MTV, and TLG (SUVmax, 13.06 ± 6.12 vs. 11.23 ± 4.77, $p = 0.01$; MTV, 554.9 ± 668.58 vs. 311.3 ± 569.21, $p < 0.001$; TLG, 2641.23 ± 3301.52 vs. 1457.38 ± 2425.98, $p < 0.001$). However, there was no significant difference in SUVmean between the expired and surviving patients (expired: 4.74 ± 1.16 vs. surviving 4.62 ± 1.11, $p = 0.35$).

Feature selection and results of survival prediction models in predicting overall survival

The top 11 features were selected for survival duration prediction using the combined model (Fig. 3). Of the evaluated TLGd and tumor organ distribution (total METAORG and high METAORG), five TLGd radiomics features were included, suggesting the importance of evaluating tumor distribution patterns for patient prognosis. Among METAORG, the axial and peripheral skeletal tumor distribution patterns, as well as the liver distribution pattern, were highly considerable predictors of overall survival. These findings indicate that organ-specific radiomic distributional features, particularly those of the metastatic axial skeleton, peripheral skeleton, and liver, were among the strongest predictors of overall survival. Among clinical factors, age group and stage (LD vs. ED) were also included in the top 11 features for predicting overall survival.

Each of these radiomics features was used to predict patient prognosis. Radiomics features #1, 2, 4, 5, and 6 showed poorer prognoses for higher radiomics values, and radiomics features # 3, 9, and 11 showed poorer prognoses for lower radiomics values (Fig. 3). To reiterate these results, for METAORG or TLGd, a shorter axis (feature #1), shorter spread (feature #2), greater variation in [^{18}F] FDG uptake (feature #4), less uniform [^{18}F] FDG uptake (feature #6), and more varied texture of the tumors (feature #11) were linked with better prognosis. For specific organs, more homogeneous [^{18}F] FDG uptake in the axial skeleton (feature #5), greater [^{18}F]FDG uptake heterogeneity in the peripheral skeleton (feature #3), and more uniform [^{18}F]FDG uptake in the liver (i.e. absence of nodular uptakes) (feature #9) were associated with better prognosis.

We then used a Cox proportional hazards model to evaluate the hazard ratio (HR) of each model as a continuous variable contributing to patient survival. All models showed a significantly higher HR for each model in predicting overall survival, with the combined model showing the highest HR of 1.009 (confidence interval [CI]: 1.005–1.012, $p < 0.001$, Table 2). Next, survival duration and event prediction model performances in the internal and external test sets for predicting patient overall survival were evaluated. In the internal test, the C-indices for the survival duration prediction model were 0.611, 0.592, 0.721, and 0.753 for the TLG, clinical, radiomics, and combined models, respectively. The other models are listed in Table 2. In the external test, the C-indices were 0.637, 0.326, 0.706, and 0.740, respectively. The combined model demonstrated the highest predictive power for both internal and external test sets. Next, we performed a Kaplan–Meier analysis using the Combined model (using the median value for stratification) to evaluate the survival duration prediction between the two groups (Supplementary Fig. 1).

For event prediction, the AUC of the combined model for both the internal and external test sets was very high (0.9472 and 0.7815, respectively; (Supplementary Fig. 2)). Other survival duration and event prediction models using TLG, clinical, and radiomics using the same methods are displayed in Supplementary Fig. 3, 4, 5, and 6.

Discussion

We showed that tumor distribution pattern is a much stronger predictor of patient prognosis than the simple tumor burden, as assessed by TLG on [^{18}F] FDG PET/CT (Fig. 4). Our findings showed that the C-index for predicting prognosis using tumor distribution radiomics analysis was markedly higher than that of clinical information

Characteristics	Internal cohort Training set ($n=291$)[a]	Internal cohort Test set ($n=73$)[b]	External cohort Test set ($n=156$)[c]	*p*-value
Mean age, years (± SD)	68.1 ± 8.6	68.8 ± 10.6	63.8 ± 10.0	**< 0.001**
				0.136[a]
				0.404[b]
				0.516[c]
Men: Women	260:31	64:9	117:39	**0.004**
				> 0.999[a]
				< 0.001[b]
				0.130[c]
Treatment method (CTx: CCRTx: IO + CTx)	151:60:80	33:13:27	156:0:0	**< 0.001**
				0.844[a]
				< 0.001[b]
				< 0.001[c]
Staging (LD: ED)	60:231	13:60	62:94	**< 0.001**
				> 0.999[a]
				< 0.001[b]
				< 0.001[c]
OS (survival: death)	45:246	11:62	44:112	**0.003**
				> 0.999[a]
				0.006[b]
				0.136[c]
Survival time, months (mean ± SD)	15.2 ± 17.1	12.8 ± 11.5	21.9 ± 28.2	**< 0.001**
				0,081[a]
				< 0.001[b]
				0.658[c]
OS rate (95% CI)				
1 year	46.6% (40.7–52.2)	38.7% (27.3–49.9)	52.7% (44.3–60.4)	0.270
2 years	19.3% (14.8–24.4)	14.8% (7.4–24.5)	28.2% (20.8–36.1)	0.066
3 years	7.9% (4.5–12.5)	4% (0.4–14.6)	20.3% (13.6–28)	**0.028**
				> 0.999[a]
				0.126[b]
				0.166[c]
PET/CT index (mean ± SD)				
SUVmax	12.58 ± 5.46	14.24 ± 5.57	12.23 ± 6.79	**0.049**
				0.098[a]
				1.000[b]
				0.051[c]
SUVmean	4.76 ± 1.15	4.95 ± 0.98	4.54 ± 1.21	**0.028**
				0.648[a]
				0.148[b]
				0.036[c]
MTV	499.97 ± 638.77	518.59 ± 673.67	518.19 ± 686.81	0.951
TLG	2407.68 ± 3152.39	2590.32 ± 3471.43	2341.84 ± 3121.53	0.859

Table 1. Patient demographics. *PET/CT* positron emission tomography/computed tomography, *TLG* total lesion glycolysis, *MTV* metabolic tumor volume, *LD* limited disease, *ED* extensive disease, *CTx* chemotherapy, *CCRTx* chemotherapy and radiotherapy, *IO + CTx* immunotherapy and chemotherapy; *OS* overall survival, *SUV* standard uptake value, *SD* standard deviation, *CI* confidence interval. Note - p-value[a]: training set vs. internal test set; p-value[b]: training set vs. external test set; p-value[c]: internal test set vs. external test set.

alone (0.721 vs. 0.592) and adding clinical data to the radiomics analysis did not notably improve the C-index (0.735 vs. 0.721). These results indicate the importance of evaluating tumor distribution in predicting prognosis. Importantly, our findings do not simply reflect the presence of distant metastasis, which is already a well-established poor prognostic factor in the TNM system. Rather, they demonstrate that the distributional pattern of metastases—such as the degree of spread, dispersion, and intra-organ involvement—provides additional prognostic information. Radiomic distributional features of metastatic axial skeleton, peripheral skeleton, and liver were identified as strong predictors of overall survival, highlighting the prognostic importance of organ-specific metastatic patterns beyond simple tumor burden. By quantifying these features through radiomics, treatment responses to chemotherapy, immunotherapy, or radiotherapy could potentially be assessed in a more

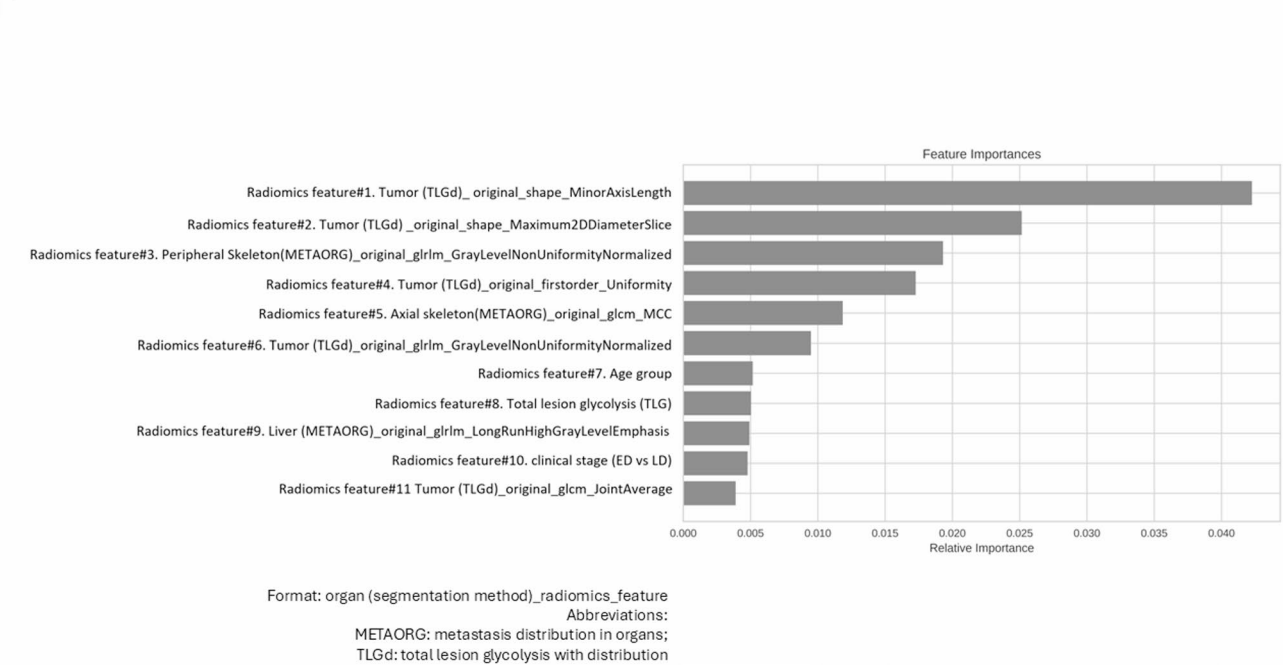

Fig. 3. Top 11 features in the combined model (conventional total lesion glycolysis [TLG] + clinical features + radiomics features) for predicting overall survival. Title Format: organ (segmentation method)_ radiomics_feature. *METAORG* metastasis distribution in organs; *TLGd* total lesion glycolysis with distribution.

Models	Internal test ($n = 73$)		External test ($n = 156$)	
	Survival duration prediction model C-index	Survival event prediction model AUC	Survival duration prediction model C-index	Survival event prediction model AUC
01. TLG	0.611	0.632	0.637	0.424
02. Clinical	0.592	0.648	0.326	0.276
03. Radiomics	0.721	0.909	0.706	0.665
04. TLG + clinical	0.648	0.853	0.584	0.475
05. TLG + radiomics	0.723	0.914	0.709	0.727
06. Clinical + radiomics	0.735	0.908	0.699	0.728
07. TLG + clinical + radiomics (Combined model)	**0.753**	**0.947**	**0.740**	**0.782**

Table 2. C-index and Cox survival analysis results for test sets. C-index, concordance index; AUC, area under the receiver operating characteristic curve; TLG, total lesion glycolysis.

objective manner, supporting broader incorporation of PET/CT into clinical treatment evaluation. The novelty of this study lies in the application of the radiomics methodology to evaluate tumor distribution patterns as a prognostic factor in SCLC. Instead of focusing on the intra-tumoral distribution pattern, as commonly done in radiomics analysis[27–30], we considered the patient as a single entity, applying radiomics to assess the overall pattern of tumor spread throughout the body.

We employed two methods to evaluate tumor distribution patterns: (1) tumor-only radiomics (TLGd), which evaluated the distribution patterns of malignant lesions throughout the patients without considering individual organ involvement; and (2) [^{18}F] FDG distribution patterns in six major organs that are prone to metastasis (METAORG), using either no cut-off or a cut-off of 2.5. The underlying premise is that these organs have a homogenous [^{18}F] FDG uptake, and tumor involvement results in a heterogeneous uptake, which may explain the strong prognostic impact of organ involvement in our study. Although individual metastatic lesions may sometimes demonstrate visually homogeneous FDG uptake, particularly in the absence of necrosis, the presence of multiple lesions within normally homogeneous organs such as the liver or skeleton produces spatial heterogeneity of FDG uptake at the organ level. This distinction highlights that our findings reflect heterogeneity across the whole organ, rather than within a single lesion. Interestingly, we observed that the tumor distribution pattern is the most important radiomics feature, as five TLGd radiomics features were included in the top 11 radiomics features. The radiomics feature of the 3D short-axis diameter (radiomics feature #1) was one of the

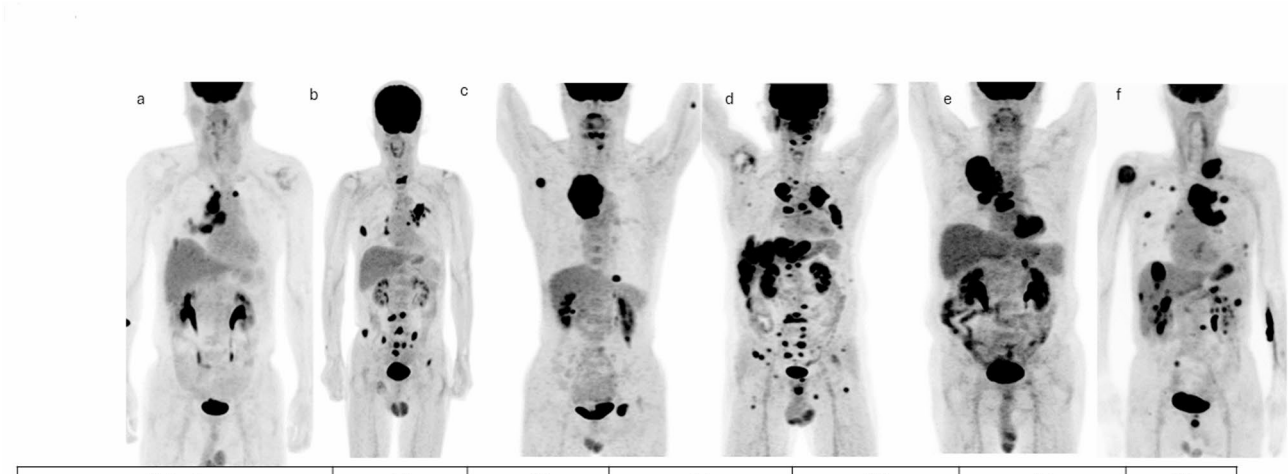

Patient	(a)	(b)	(c)	(d)	(e)	(f)
TLG	664.2	650	2724.2	2661.9	2468.4	2447.1
METAORG (minor_axis)	87.7	211.4	85.2	208.3	76.7	294.4
Survival time (months)	53.9	5.0	15	1.5	18.4	1.3

Fig. 4. Representative images of radiomics (METAORG) demonstrating better stratification of overall survival compared to that with conventional TLG. (**a**, **b**) Significant differences in overall survival time (OS) in patients with similar tumor volumes (TLG 664 vs. 650 cm^3). (**a**) A 67-year-old man with a short minor axis value (87.7) and a longer OS (54 months) compared with (**b**) a 76-year-old man with a long minor axis value (211.4) and a shorter OS of 5 months. (**c**, **d**) High tumor burden with a TLG value of 2,724 vs. 2,661 cm^3. (**c**) A 55-year-old man with a short minor axis value (85.2) and a longer OS (15 months) compared with (**d**) a 67-year-old man with a long minor axis value (208.3) and a shorter OS of 1.5 months. (**e**, **f**) High tumor burden with a TLG value of 2,468 vs. 2,447 cm^3 (**e**) A 75-year-old man with a short minor axis value (76.7) and a longer OS (18 months) compared with (**f**) a 78-year-old man with a long minor axis value (294) and a shorter OS (1.3 months). *METAORG* metastasis distribution in organs, *TLG* total lesion glycolysis.

strongest prognostic indices in our patient population. In classical radiomics, the short-axis diameter is a first-order feature and is defined as the shortest length of the lesion. As we applied radiomics to evaluate whole-body tumor distribution patterns, the 3D short-axis diameter reflected the distance between individual malignant lesions, aligning well with the current understanding that greater tumor distribution in the body is a poor prognosis factor[17,19,31,32]. Similarly, a shorter tumor spread pattern, as indicated by radiomics, associated with better prognosis also supports existing assumptions regarding metastasis patterns and prognosis. We also found that patients with greater variation in [^{18}F] FDG uptake intensity across all segmented tumor voxels (features #4 and 6), and more heterogeneous spatial texture within the segmented tumors (feature #11), had better prognosis. These three radiomics features suggest that increased variability in [^{18}F] FDG uptake is linked to an improved prognosis. However, further studies are needed to validate these results and explore the underlying reasons for this relationship. Regardless, the major clinical application of this METAORG methodology is automatic quantification of metastasis distribution in multiple organs, which may provide clinicians with numerical values for metastasis sub-stratification, treatment response assessment, and survival analysis prediction.

Our organ-specific radiomics features (i.e., organ-based tumor distribution: METAORG) align well with the current understanding that liver and bone metastasis are poor prognostic factors in SCLC[12,13,32,33]. Of the six organs evaluated, we showed that skeletal and liver metastases were the major organs influencing patient prognosis, which is concordant with the findings of multiple meta-analyses[32,34]. Not only do these two organs heavily influence survival, [^{18}F] FDG uptake patterns in the skeleton and liver also play a critical role. Interestingly, we observed contrasting [^{18}F] FDG uptake patterns in the two skeleton groups: homogeneous [^{18}F] FDG uptake in the axial skeleton and heterogeneous [^{18}F] FDG uptake in the peripheral skeleton were associated with better patient survival. Further studies are required to evaluate the contrasting skeletal features.

The implications of our study suggest that CT-based radiomics feature extraction from PET images could significantly simplify the evaluation of patient prognosis and become an important tool for clinicians. Automated CT-based delineation can substantially reduce the labor-intensive process of tumor delineation. Moreover, by relying on automated CT-based organ segmentation and radiomics quantification, our approach enables the standardization of FDG evaluation, reducing inter-observer variability and enabling more consistent prognostic assessment across patients and institutions. Although using a simple 2.5 SUV cut-off for tumor delineation may lead to gross errors, we believe that a holistic evaluation of [^{18}F] FDG uptake patterns is more important than precise evaluation of individual tumors. Nevertheless, we found that tumor-only distribution patterns using manual VOI delineation are more substantial than specific organ involvement patterns or conventional TLG for SCLC and that modifying CT-based organ VOIs by determining optimal cut-off values could greatly simplify

the current [^{18}F] FDG PET/CT evaluation methods for manually delineating individual tumors for prognostic evaluation.

Despite these limitations, semi-automatic delineation of multiple organs using CT-based VOI may enhance the accessibility and applicability of PET/CT scan analysis for clinicians, requiring minimal manual effort to identify individual tumors. For example, this method may be used as an automatic screening tool to approximate the tumor burden in multiple organs and provide clinicians with a semi-automatic prognostic metric (such as a nomogram) for patient prognosis. Another potential application is in the prediction of chemotherapy response, as current methods only evaluate tumor size and metabolism.

Beyond prognostic performance, our approach may also have broader clinical utility. By integrating tumor burden with distributional patterns through the METAORG methodology, it provides a quantifiable index that could complement or surpass RECIST, which is limited to tumor burden alone. Such an approach may support more refined treatment stratification, allowing high-risk patients to be identified for intensified or tailored therapeutic strategies. Prospective validation will be required to confirm this potential in clinical practice.

Our study has some limitations. First, potential bias may have been introduced due to differences in scanner vendors and acquisition parameters, as our cohort included PET/CT scans acquired on both GE and Siemens systems. Nevertheless, the robustness of our models across these heterogeneous conditions suggests that the proposed approach may be generalizable, although scanner- and parameter-related variability remains a limitation. Second, we assumed that tumors were defined as having an SUV > 2.5. Given that SCLC is generally highly glycolytic, we surmise that this is a safe assumption, and the method will likely be sufficient for highly glycolytic tumors, such as lymphoma or squamous cell pathologies. In our cohort, this threshold was sufficient to capture the vast majority of lesions, although a few necrotic or very small lesions may have been underestimated. Importantly, the METAORG methodology, which evaluates organ-level distributional patterns, mitigates the effect of such segmentation inaccuracies. We also acknowledge that this approach may not be applicable to malignancies with inherently low FDG avidity (e.g., thyroid cancer, renal cell carcinoma, or mucinous tumors). Third, treatment modalities were not explicitly adjusted for in the survival models. However, disease stage (LD vs. ED), which is strongly correlated with treatment modality, was considered in the analysis, and SCLC management is generally standardized with systemic chemotherapy as the backbone of treatment. Thus, variability attributable to treatment modality is expected to be less pronounced than in other malignancies. Nevertheless, treatment effects may still act as potential confounders, and future studies should incorporate treatment covariates to further validate the robustness of our findings. Fourth, histologic confirmation of all metastatic lesions was not feasible in this retrospective cohort, and thoracic lymph node assessment was performed without contrast-enhanced CT. These factors may have introduced potential misclassification; however, metastatic involvement was determined based on consensus PET/CT interpretation and supported by clinical follow-up. Fifth, the higher survival observed in the external validation cohort despite chemotherapy-only treatment likely reflects demographic differences and potential selection bias, as these patients were younger and had a higher proportion of limited disease compared with the internal cohort. This emphasizes that survival comparisons between cohorts should be interpreted with caution. This finding indicates that the apparent survival advantage in the external cohort may primarily reflect differences in patient characteristics rather than therapeutic efficacy. Sixth, current CT-based artificial intelligence segmentation methods do not incorporate mediastinal lymph nodes, and METAORG does not include mediastinal lymph node as a separate organ. However, we manually drew the regions of interest on the mediastinal lymph nodes to be included in TLGd. Further methodological development is required to include mediastinal structures in the METAORG methodology. Finally, we used CT-based organ VOIs and overlaid these VOIs on PET images, which may be problematic in areas of increased motion, such as the lung base, liver, and spleen. However, because the same CT scan is used for attenuation correction, SUV measurements are likely to be consistently over- or under-represented. In addition, exophytic tumor involvement may be miscategorized for other organs, as the current TotalSegmentator is used for non-malignant organs. Therefore, further development is needed to accurately delineate tumor organ involvement before the automatic assessment of tumor distribution.

In conclusion, we demonstrated that applying the radiomics method to whole-body malignant lesions has clinical applications in predicting SCLC prognosis and potentially to other [^{18}F] FDG-avid malignancies. Our findings indicate that the tumor spread pattern is more substantial than the simple tumor burden or clinical factors. This method has the potential to provide clinicians with a semi-automatic, unified numerical metric for malignancy, with applications for treatment response and patient prognosis.

Data availability

The datasets generated during and/or analyzed during the current study are available from the corresponding author on reasonable request.

Received: 12 February 2025; Accepted: 8 October 2025
Published online: 14 November 2025

References

1. Siegel, R. L., Miller, K. D., Fuchs, H. E. & Jemal, A. Cancer Statistics, 2021. *CA Cancer J. Clin.* **71**, 7–33 (2021).
2. Xia, C. et al. Cancer statistics in China and united States, 2022: profiles, trends, and determinants. *Chin. Med. J. (Engl).* **135**, 584–590 (2022).
3. Bray, F. et al. Global cancer statistics 2022: GLOBOCAN estimates of incidence and mortality worldwide for 36 cancers in 185 countries. *CA Cancer J. Clin.* (2024).
4. Calles, A., Aguado, G., Sandoval, C. & Alvarez, R. The role of immunotherapy in small cell lung cancer. *Clin. Transl Oncol.* **21**, 961–976 (2019).

5. Chaffer, C. L. & Weinberg, R. A. A perspective on cancer cell metastasis. *Science* **331**, 1559–1564 (2011).
6. Combs, S. E. et al. Bolstering the case for lobectomy in stages I, II, and IIIA small-cell lung cancer using the National cancer data base. *J. Thorac. Oncol.* **10**, 316–323 (2015).
7. Kahnert, K., Kauffmann-Guerrero, D. & Huber, R. M. SCLC-State of the Art and what does the future have in store? *Clin. Lung Cancer*. **17**, 325–333 (2016).
8. Schwendenwein, A. et al. Molecular profiles of small cell lung cancer subtypes: therapeutic implications. *Mol. Ther. Oncolytics*. **20**, 470–483 (2021).
9. Tariq, S., Kim, S. Y., Monteiro de Oliveira Novaes, J. & Cheng, H. Update 2021: management of small cell lung cancer. *Lung* **199**, 579–587 (2021).
10. Wang, Y. et al. Development and validation of a prognostic model of resectable small-cell lung cancer: a large population-based cohort study and external validation. *J. Transl Med.* **18**, 237 (2020).
11. Tian, Y. et al. Potential immune escape mechanisms underlying the distinct clinical outcome of immune checkpoint Blockades in small cell lung cancer. *J. Hematol. Oncol.* **12**, 67 (2019).
12. Li, J. et al. Prognostic value of site-specific metastases in lung cancer: A population based study. *J. Cancer*. **10**, 3079–3086 (2019).
13. Nakazawa, K. et al. Specific organ metastases and survival in small cell lung cancer. *Oncol. Lett.* **4**, 617–620 (2012).
14. Milovanovic, I. S., Stjepanovic, M. & Mitrovic, D. Distribution patterns of the metastases of the lung carcinoma in relation to histological type of the primary tumor: an autopsy study. *Ann. Thorac. Med.* **12**, 191–198 (2017).
15. Popper, H. H. Progression and metastasis of lung cancer. *Cancer Metastasis Rev.* **35**, 75–91 (2016).
16. Budczies, J. et al. The landscape of metastatic progression patterns across major human cancers. *Oncotarget* **6**, 570–583 (2015).
17. Gorka, E. et al. Distance from primary tumor is the strongest predictor for early onset of brain metastases in melanoma. *Anticancer Res.* **36**, 3065–3069 (2016).
18. Sasaki, K. et al. The tumor burden score: A new Metro-ticket prognostic tool for colorectal liver metastases based on tumor size and number of tumors. *Ann. Surg.* **267**, 132–141 (2018).
19. Kawamoto, N. et al. Tumor distance from the mediastinum predicts N2 upstaging in clinical stage I lower-lobe non-small cell lung cancer. *J. Thorac. Cardiovasc. Surg.* **167**, 488–497 (2024). e482.
20. Suh, Y. J. et al. Computed tomography radiomics for preoperative prediction of spread through air spaces in the early stage of surgically resected lung adenocarcinomas. *Yonsei Med. J.* **65**, 163–173 (2024).
21. Hong, G. S. et al. Overcoming the challenges in the development and implementation of artificial intelligence in radiology: A comprehensive review of solutions beyond supervised learning. *Korean J. Radiol.* **24**, 1061–1080 (2023).
22. Li, H. J. et al. *Radiomics-based Support Vector Machine Distinguishes Molecular Events Driving Progression of Lung Adenocarcinoma* (J Thorac Oncol, 2024).
23. Shiyam Sundar, L. K. et al. Fully Automated, semantic segmentation of Whole-Body (18)F-FDG PET/CT images based on Data-Centric artificial intelligence. *J. Nucl. Med.* **63**, 1941–1948 (2022).
24. Fedorov, A. et al. 3D slicer as an image computing platform for the quantitative imaging network. *Magn. Reson. Imaging*. **30**, 1323–1341 (2012).
25. D'Antonoli, T. A. et al. TotalSegmentator MRI: Sequence-Independent segmentation of 59 anatomical structures in MR images. (2024). arXiv preprint arXiv:2405.19492.
26. Wasserthal, J. et al. TotalSegmentator: robust segmentation of 104 anatomic structures in CT images. *Radiol. Artif. Intell.* **5**, e230024 (2023).
27. Chang, H. et al. Prognostic significance of metabolic parameters measured by (18)F-FDG PET/CT in limited-stage small-cell lung carcinoma. *J. Cancer Res. Clin. Oncol.* **145**, 1361–1367 (2019).
28. Mirili, C. et al. Prognostic significance of neutrophil/lymphocyte ratio (NLR) and correlation with PET-CT metabolic parameters in small cell lung cancer (SCLC). *Int. J. Clin. Oncol.* **24**, 168–178 (2019).
29. Sachpekidis, C. et al. Application of an artificial intelligence-based tool in [(18)F]FDG PET/CT for the assessment of bone marrow involvement in multiple myeloma. *Eur. J. Nucl. Med. Mol. Imaging*. **50**, 3697–3708 (2023).
30. Kim, S. et al. Prediction of microsatellite instability in colorectal cancer using a machine learning model based on PET/CT radiomics. *Yonsei Med. J.* **64**, 320–326 (2023).
31. Klikovits, T. et al. New insights into the impact of primary lung adenocarcinoma location on metastatic sites and sequence: A multicenter cohort study. *Lung Cancer*. **126**, 139–148 (2018).
32. Ren, Y. et al. Prognostic effect of liver metastasis in lung cancer patients with distant metastasis. *Oncotarget* **7**, 53245–53253 (2016).
33. Cai, H. et al. The prognostic analysis of different metastatic patterns in extensive-stage small-cell lung cancer patients: a large population-based study. *Future Oncol.* **14**, 1397–1407 (2018).
34. Wu, Y. et al. Prognostic factors in extensive-stage small cell lung cancer patients with organ-specific metastasis: unveiling commonalities and disparities. *J. Cancer Res. Clin. Oncol.* **150**, 74 (2024).

Acknowledgements

This work was supported by multiple grants: an NRF grant funded by the Korean government (NRF-2022R1F1A1071702) awarded to Y.H.L; A research grant of Yonsei University College of Medicine (1-2022-0017) awarded to Y.H.L. A grant from the Korea Health Technology R&D Project through the Korea Health Industry Development Institute (KHIDI), funded by the Ministry of Health & Welfare, the Republic of Korea (grant number: HR18C001208) awarded to A.C.; and another NRF grant funded by the Korean government (NRF- 2022R1A2C2092016) also awarded to A.C.

Author contributions

Conceptualization: Arthur Cho and Young Han Lee; Methodology: Jiwoo Park, Young Han Lee; Formal analysis: Jiwoo Park, Soo Ho Ahn; Data Curation: Jae-Hoon Lee and Arthur Cho; Writing: Jiwoo Park, Arthur Cho, Young Han Lee; Review & Editing: All authors; Supervision: Arthur Cho and Young Han Lee; Funding acquisition: Arthur Cho and Young Han Lee.

Funding

This work was supported by multiple grants: an NRF grant funded by the Korean government (NRF-2022R1F1A1071702) awarded to Y.H.L. A research grant of Yonsei University College of Medicine (1-2022-0017) awarded to Y.H.L. A grant from the Korea Health Technology R&D Project through the Korea Health Industry Development Institute (KHIDI), funded by the Ministry of Health & Welfare, the Republic of Korea (grant number: HR18C001208) awarded to A.C.; and another NRF grant funded by the Korean government (NRF- 2022R1A2C2092016) also awarded to A.C.

Declarations

Competing interests
The authors declare no competing interests.

Ethics approval and consent to participate
Due to the retrospective nature of the study, The Institutional Review Board of Yonsei University's Health System waived the need of obtaining informed consent. All methods were carried out in accordance with relevant guidelines and regulations. The study was conducted in compliance with the Declaration of Helsinki. The authors have complete control of the data and information submitted for publication.

Additional information
Correspondence and requests for materials should be addressed to Y.H.L. or A.C.

Reprints and permissions information is available at www.nature.com/reprints.

Publisher's note Springer Nature remains neutral with regard to jurisdictional claims in published maps and institutional affiliations.